Supporting information

Halide bridged trinuclear rhodium complexes and their inhibiting influence in catalysis.

Angelika Preetz[a], Christina Kohrt[a], Antje Meißner[a], Siping Wei[a], Hans-Joachim Drexler[a], Helmut Buschmann[b], D. Heller[a,*]

[a]Leibniz-Institut für Katalyse e.V. an der Universität Rostock, Albert-Einstein-Straße 29a, 18059, Rostock, Germany. E-mail: detlef.heller@catalysis.de; Fax: (+49) 381-1281-51183; Tel: (+49) 381-1281-183.

[b]Pharmaconsulting Aachen, Ludwigsallee 21, 052062 Aachen, Germany. E-mail: h.buschmann@pharma-consulting-aachen.de.

Table of contents

1. **Chemical structures of applied ligands**
2. **NMR spectra and hydrogen consumption curves**
3. **Crystallographic Data**

1. Chemical structures of applied ligands

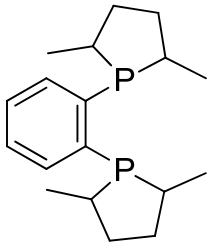

1,2-Bis(2,5-dimethylphospholano)benzene
(Me-DuPHOS)

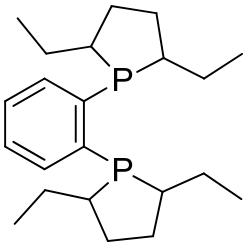

1,2-Bis(2,5-diethylphospholano)benzene
(Et-DuPHOS)

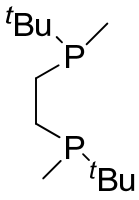

1,2-Bis(t-butyl(methyl)phosphino)ethane
(t-Bu-BisP*)

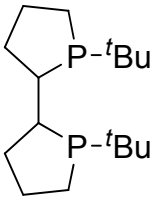

1,1'-Di-t-butyl-(2,2')-diphospholane
(Tangphos)

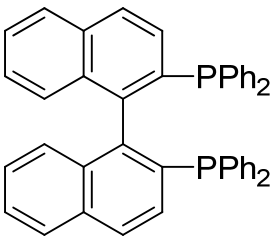

2,2'-Bis(diphenylphosphino)-1,1'-
binaphthyl (BINAP)

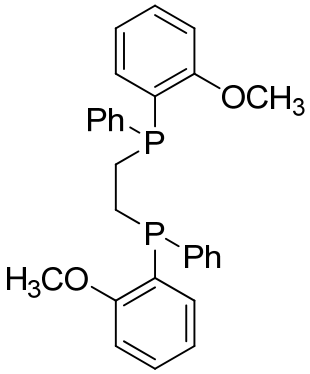

1,2-Bis(*o*-methoxy-phenylphosphino)-
ethane (DIPAMP)

2. NMR spectra and hydrogen consumption curves

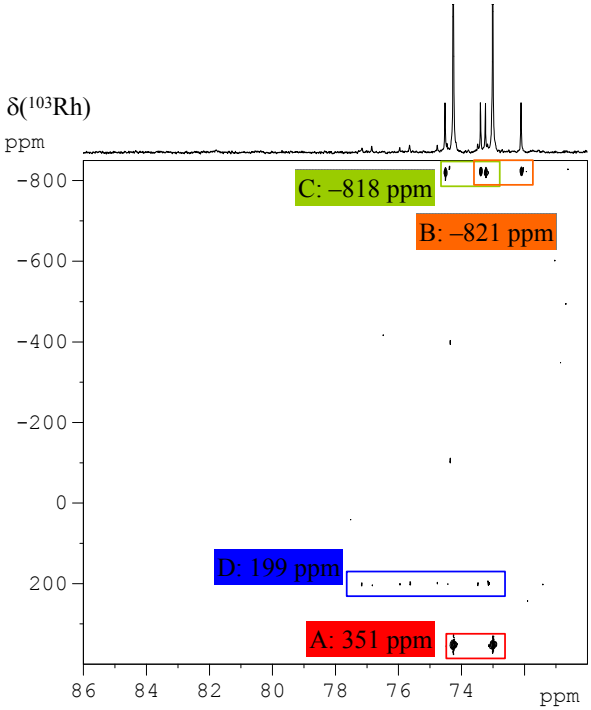

Diastereomeric couple of arene complexes (B,C)

C:[Rh(DIPAMP)(arene)][BF_4]
δ(^{31}P) 73.9 ppm ($J_{P\text{-}Rh}$=208 Hz)

B: [Rh(DIPAMP)(arene)][BF_4]
δ(^{31}P) 72.8 ppm ($J_{P\text{-}Rh}$=208 Hz)

D:[Rh_3(DIPAMP)$_3$(OMe)(OH)][BF_4]
δ(^{31}P) 76.4 ppm ($J_{P\text{-}Rh}$=195 Hz,
74.0 ppm ($J_{P\text{-}Rh}$=208 Hz)

A: [Rh_3(DIPAMP)$_3$($OMe)_2$][BF_4]
δ(^{31}P) 73.6 ppm ($J_{P\text{-}Rh}$=202Hz)

Figure S 1: ^{31}P-^{103}Rh-correlation spectrum of a mixture of the solvate complex [Rh(DIPAMP)(MeOH-d_4)$_2$][BF_4] (0.02 mmol) and 100μl [2-(3-methoxy-phenyl)-cyclohex-1-enylmethyl]-dimethylamine (0.4 mmol). The signals highlighted in red and purple correspond to the (μ_3-OMe)$_2$ and (μ_3-OMe)(μ_3-OH) bridged trinuclear complexes (75 %), the signals highlighted in green and orange are due to diastereomeric arene complexes (25 %). The substrate (purity of > 99 %) contains traces of water which lead to the formation of the mixed trinuclear complex.

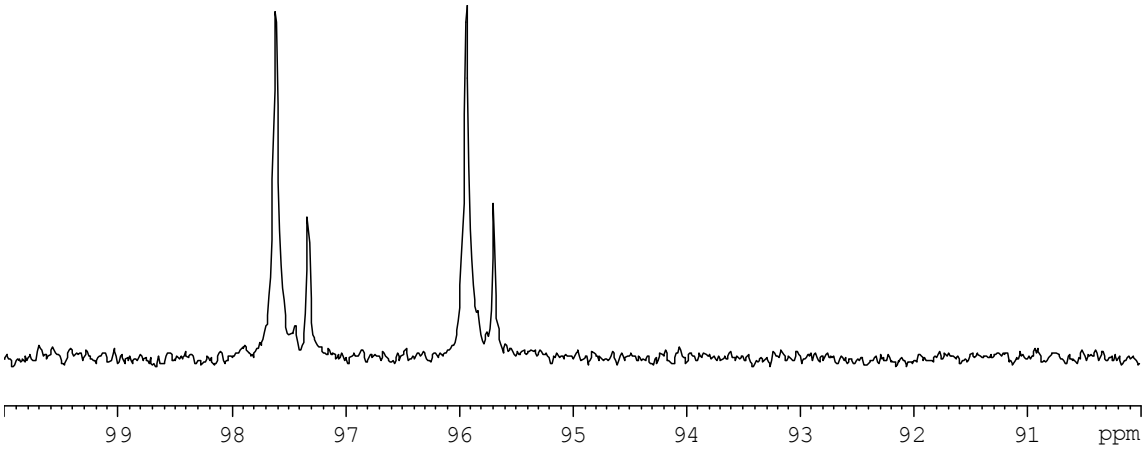

Figure S 2: ^{31}P{^{1}H}-NMR spectrum of a mixture of [Rh(Me-DuPHOS)(μ_2-Cl)]$_2$ and [Rh(Me-DuPHOS)(MeOH)$_2$][BF_4] dissolved in MeOH / THF (1:1). Both complexes, the trinuclear complex [Rh_3(MeDuPHOS)$_3$(μ_3-Cl)$_2$][BF_4] (78 %, MeOH-d_4, δ = 96.8 ppm, $J_{P\text{-}Rh}$ = 204.7 Hz) and the dinuclear complex [Rh(MeDuPHOS)(μ_2-Cl)]$_2$ (MeOD-d_4, δ = 96.5, $J_{P\text{-}Rh}$ = 198.3 Hz) can be found in solution.

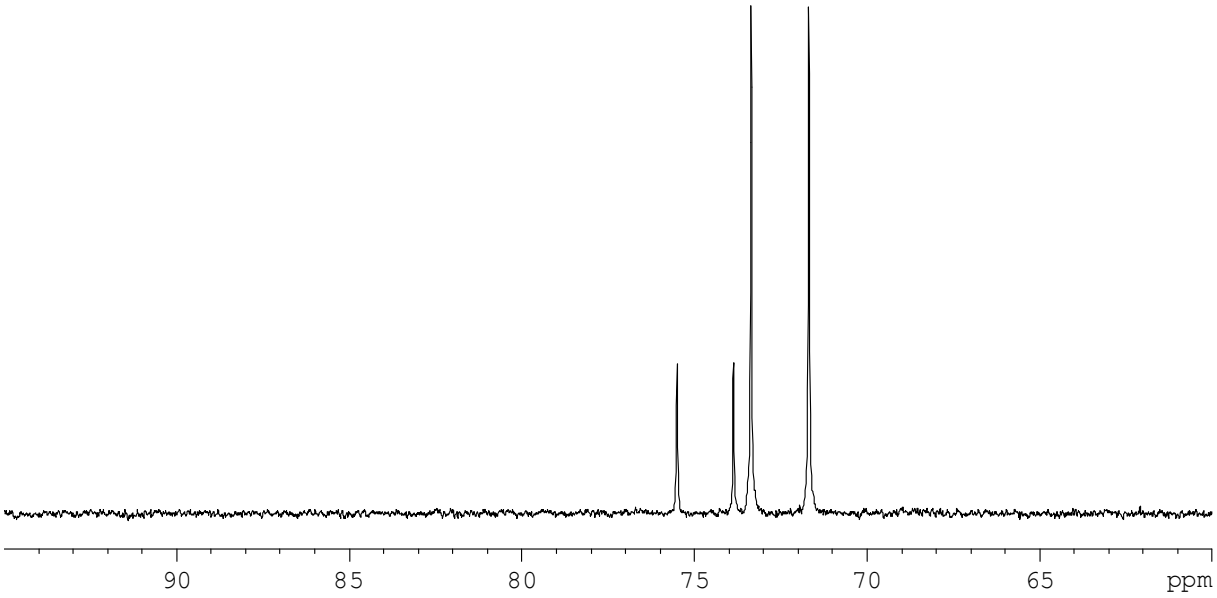

Figure S 3a: $^{31}P\{^{1}H\}$-NMR spectrum of a mixture of [Rh(DIPAMP)(MeOH-d_4)$_2$][BF_4] (0.01 mmol) and NaCl (0.04 mmol) in MeOH-d_4.

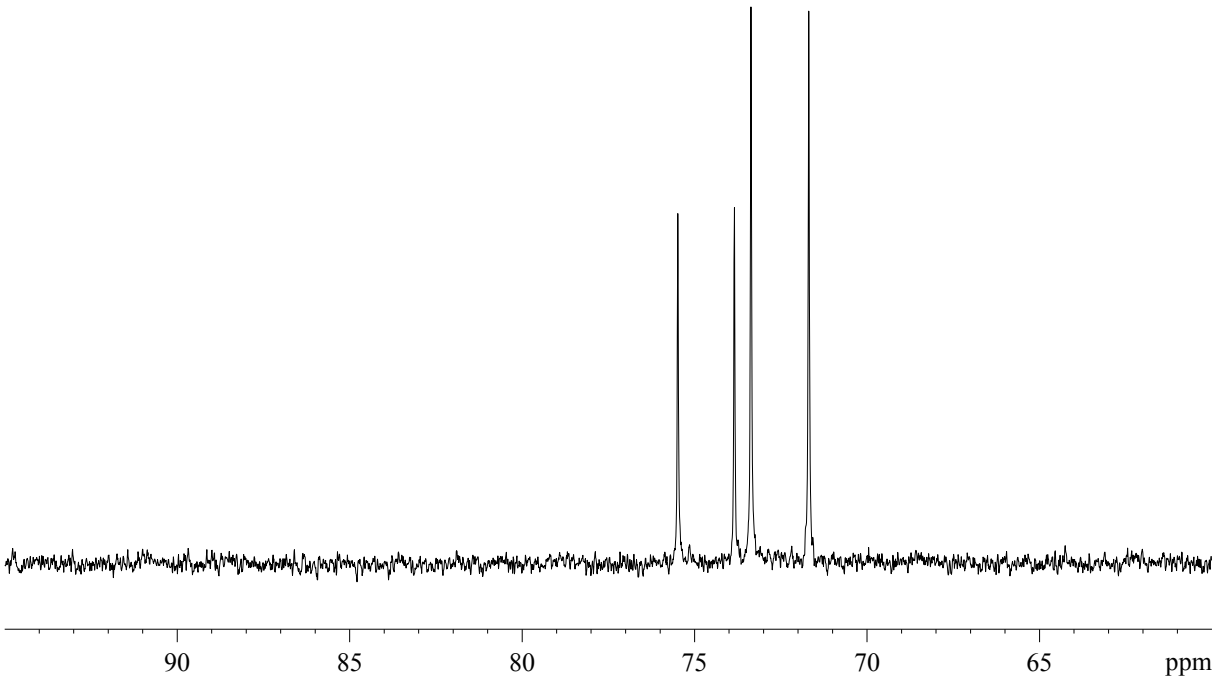

Figure S 3b: $^{31}P\{^{1}H\}$-NMR spectrum of a mixture of [Rh(DIPAMP)(MeOH-d_4)$_2$]BF_4 (0,01 mmol) and 0,34 mmol NaCl in MeOH-d_4. The observed integral ratio of dinuclear to trinuclear complex is 37:63.

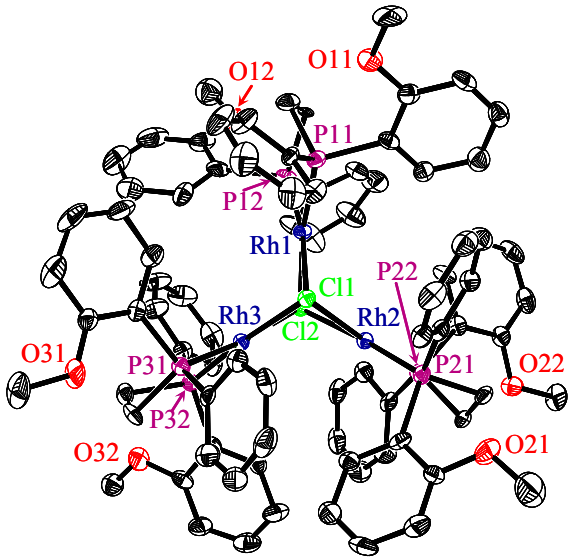

Figure S 4: Molecular structure of the cation in $[Rh_3((R,R)\text{-DIPAMP})_3(\mu_3\text{-Cl})_2][BF_4]$; ORTEP, 30 % probability ellipsoids. Hydrogen atoms of the ligand were omitted for clarity. Selected distances [Å] and angles [°]: Rh-Rh 3.128-3.197(2), Rh-P 2.179-2.189(3), Rh-Cl 2.419-2.438(3), P-Rh-P 84.8-85.2(2), Cl-Rh-Cl 82.0-82.5(1).

The $^{31}P\{^1H\}$-NMR spectrum of the dissolved crystals shows a doublet (δ 72.5 ppm, $J_{P\text{-}Rh}$ = 203.5 Hz), which is similar to that of the OMe-bridged trinuclear complex $[Rh_3(DIPAMP)_3(\mu_3\text{-OMe})_2][BF_4]$.

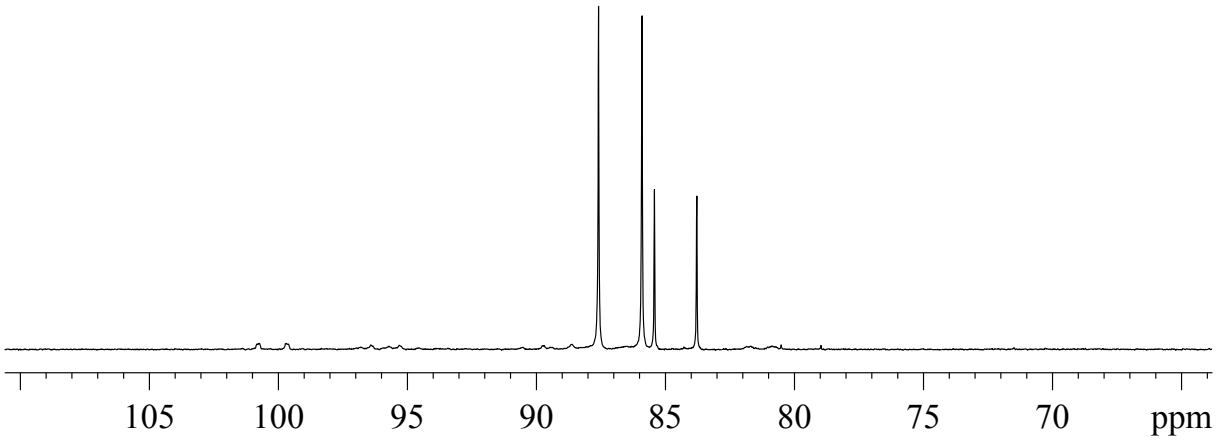

Figure S 5: $^{31}P\{^1H\}$-NMR spectrum of the solvate complex $[Rh(t\text{-Bu-BisP*})(MeOH\text{-}d_4)_2][BF_4]$ and NaCl in MeOH-d_4.

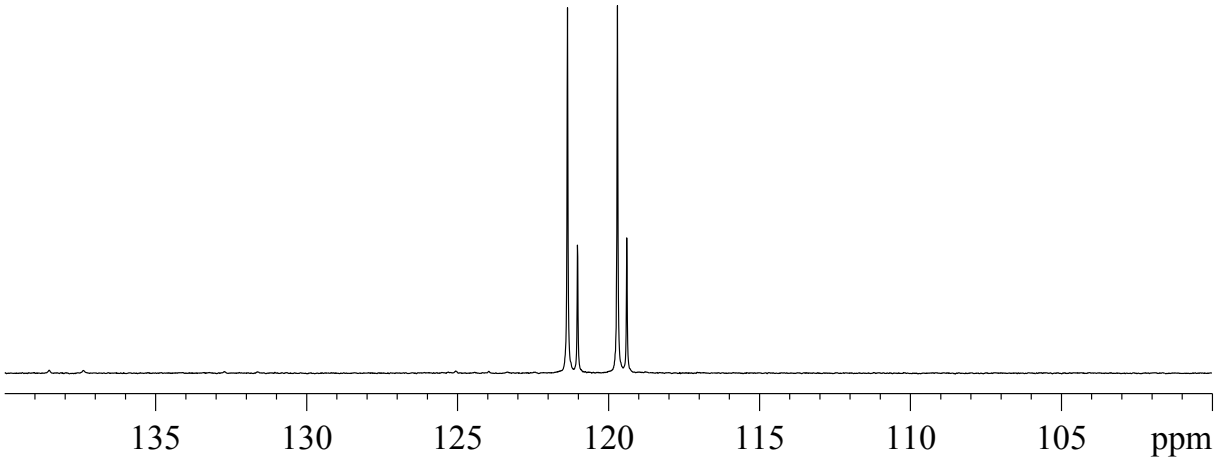

Figure S 6: $^{31}P\{^{1}H\}$-NMR spectrum of the solvate complex [Rh(Tangphos)(MeOH-d_4)$_2$][BF_4] and NaCl in MeOH-d_4.

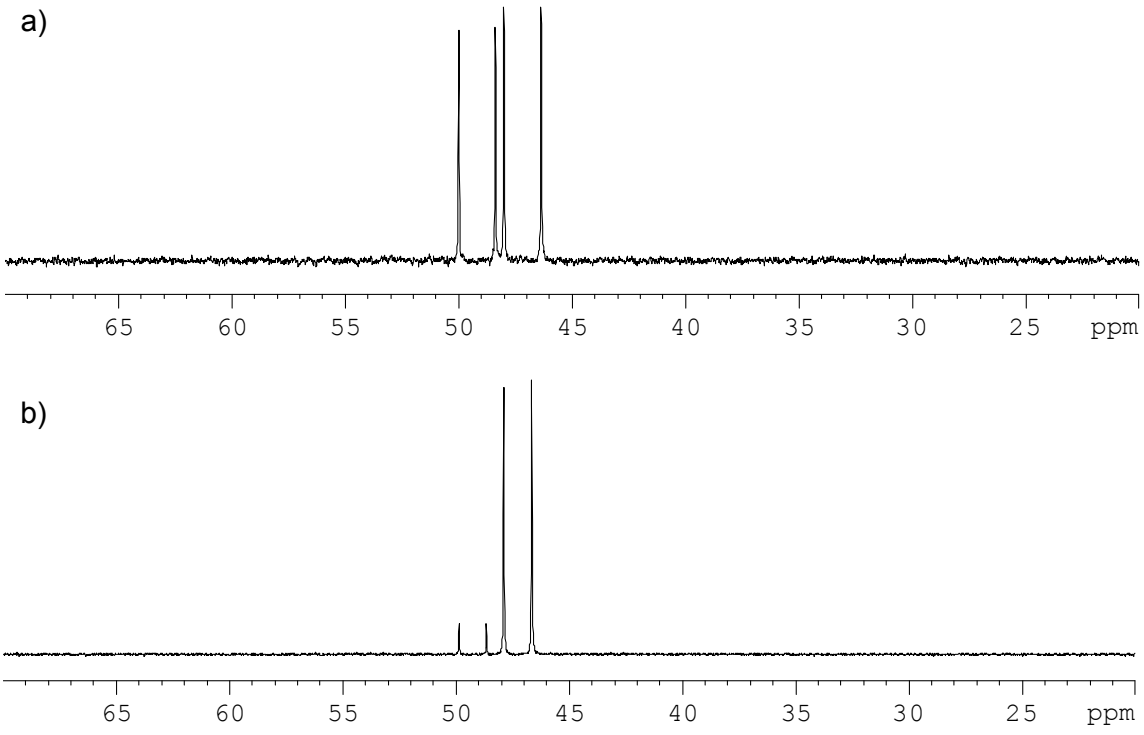

Figure S 7: $^{31}P\{^{1}H\}$-NMR spectra of reaction mixtures of [Rh(BINAP)(MeOH-d_4)$_2$][BF_4] and NaCl in MeOH-d_4/CH_2Cl_2 with two different ratios: a) Rh:Cl = 1:2 and b) Rh:Cl = 3:2.

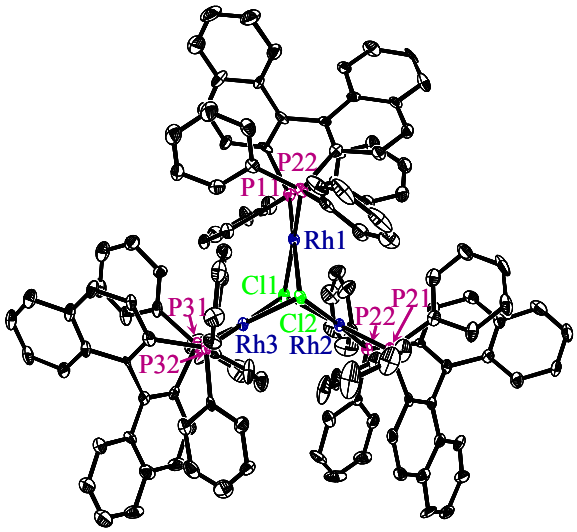

Figure S 8: Molecular structure of the cation in $[Rh_3((R)\text{-BINAP})_3(\mu_2\text{-Cl})_2][OTf]$; ORTEP, 30 % probability ellipsoids. Hydrogen atoms of the ligand were omitted for clarity. Selected distances [Å] and angles [°]: Rh-Rh: 3.258-3.294(2), Rh-P: 2.202-2.226(2), Rh-Cl: 2.422-2.436(2), P-Rh-P: 89.8 – 90.2(1), Cl-Rh-Cl: 77.7 – 77.9(1).

The μ_2-chloro-bridged trinuclear complex $[Rh_3((R)\text{-BINAP})_3(\mu_2\text{-Cl})_2][OTf]$ was isolated during experiments in which we tried to crystallize a catalyst-substrate complex with the ligand BINAP. Attempts to recrystallize the catalyst-substrate complex from CH_2Cl_2 failed. Instead, the trinuclear complex was obtained; the solvent CH_2Cl_2 must have been the source of chloride.

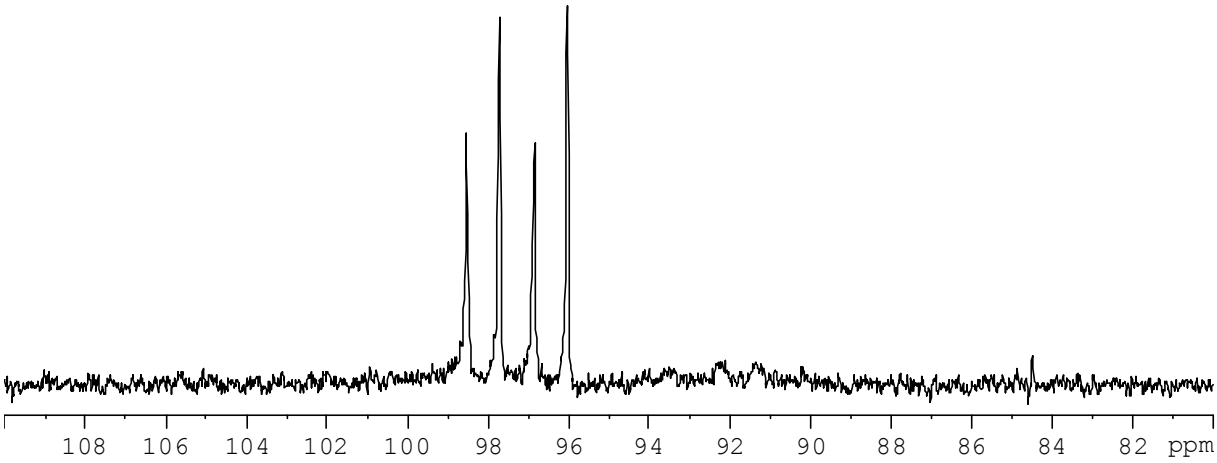

Figure S 9: $^{31}P\{^1H\}$-NMR spectrum of a mixture of $[Rh(MeDuPHOS)(\mu_2\text{-Br})]_2$ (δ = 97.7 ppm, $J_{P\text{-}Rh}$ = 202.2 Hz) and $[Rh_3(MeDuPHOS)_3(\mu_3\text{-Br})_2][BF_4]$ (δ = 96.9 ppm, $J_{P\text{-}Rh}$ = 204.7 Hz) in CH_2Cl_2-d_2.

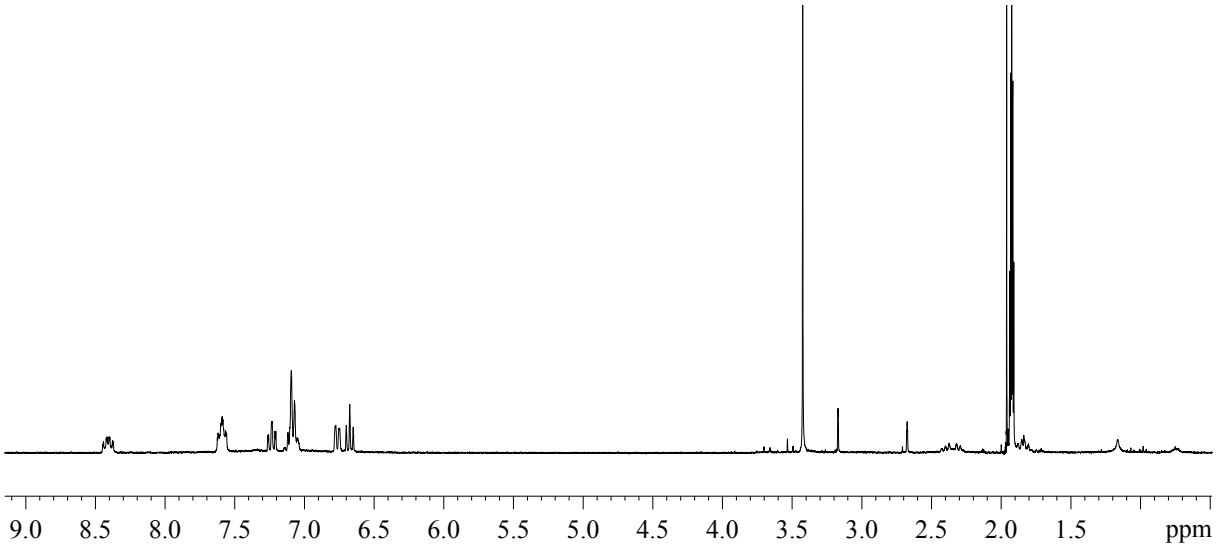

Figure S 10: ^{1}H-NMR spectrum of $[Rh_2(DIPAMP)_2(\mu_2\text{-}Br)_2]$ in acetone-d_6.

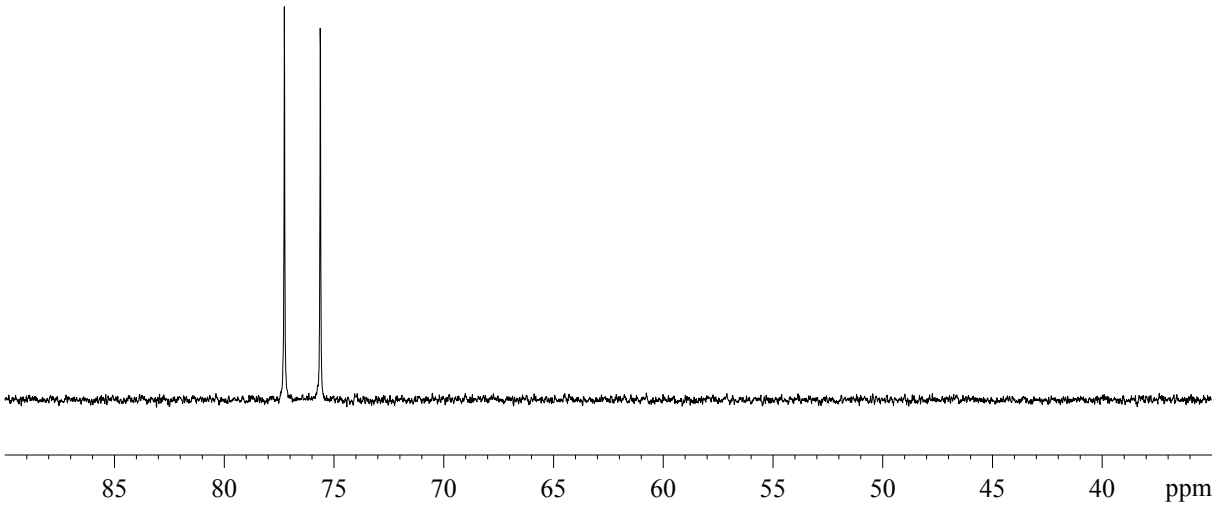

Figure S 11: $^{31}P\{^{1}H\}$-NMR spectrum of $[Rh_2(DIPAMP)_2(\mu_2\text{-}Br)_2]$ in acetone-d_6.

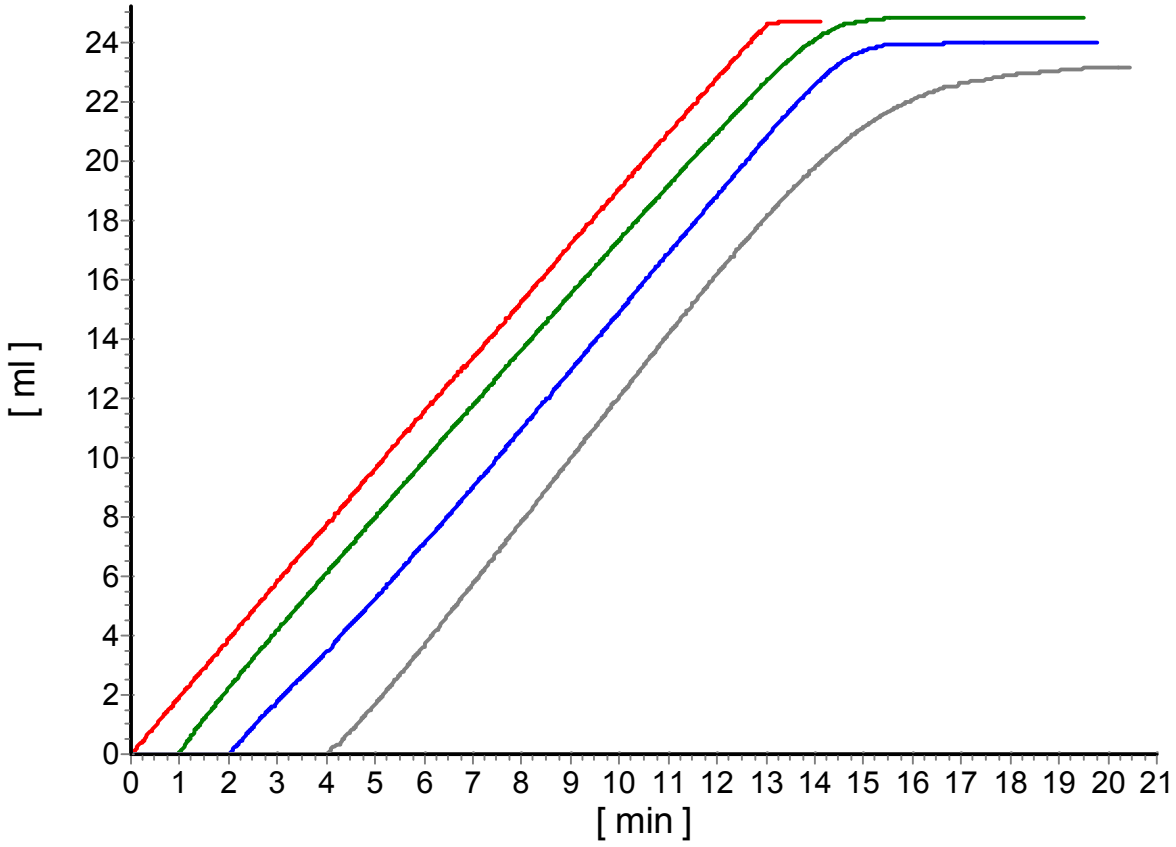

Figure S 12: Hydrogen consumption curves for the catalytic hydrogenation of 1.0 mmol methyl acetylaminocinnamate (mac) with 0.01 mmol $[Rh(DIPAMP)(MeOH)_2][BF_4]$ in the presence of different amounts of NaCl: no NaCl (red); 0.1 mmol NaCl together with 1.0 mmol substrate in a glass ampoule (green), 0.1 mmol NaCl together with the catalyst (blue), 1.0 mmol NaCl together with the catalyst (grey); 15.0 ml MeOH, 25 °C and 1.01 bar pressure. The green, blue and grey curves are time-delayed for clarity.

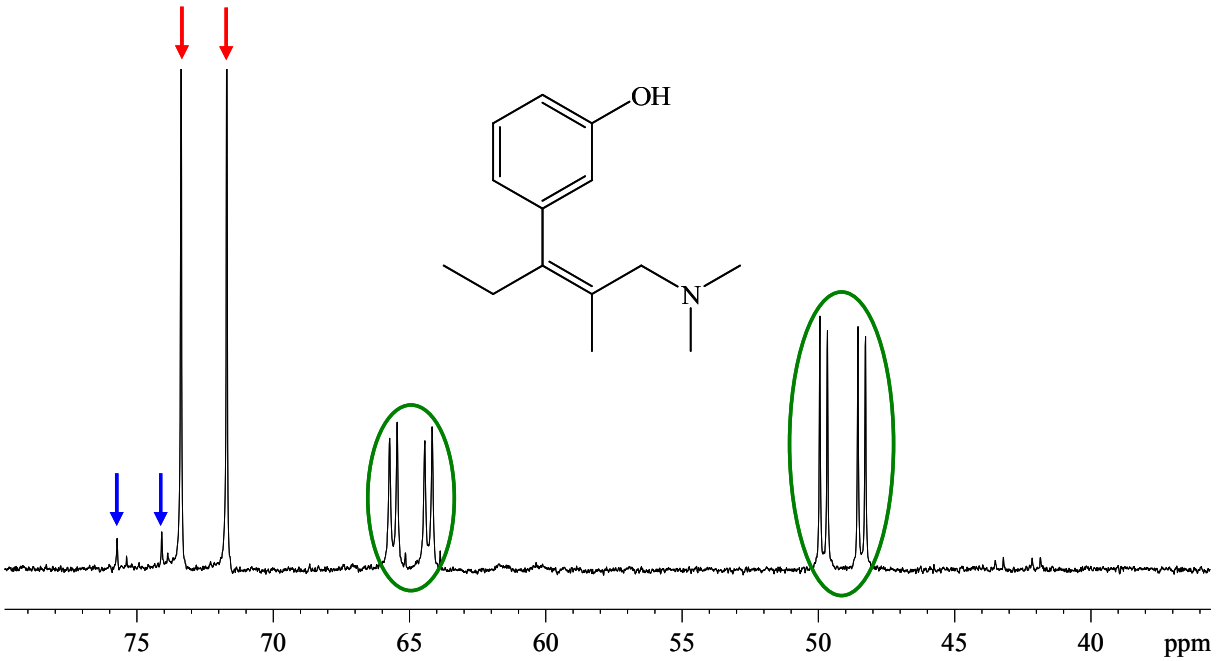

Figure S 13: $^{31}P\{^{1}H\}$-NMR spectrum of a solution of [Rh(DIPAMP)(MeOH-d_4)$_2$][BF_4] and (3-[(2*R*,3*S*)-1-(dimethylamino)-2-methylpentan-3-yl]phenol (molar ratio Rhodium: substrate = 1:10). About 34 % of the signal intensity (red arrows) correspond to the doublet of the trinuclear complex [Rh_3(DIPAMP)$_3$(μ_3-Cl)$_2$][BF_4]. The signal set highlighted with blue arrows (2 % of signal intensity, δ (MeOH-d_4) = 74.9 ppm ($J_{P\text{-}Rh}$ = 198.9 Hz)) fits with the coupling and chemical shift found for the dinuclear complex [Rh_2(DIPAMP)$_2$(μ_2-Cl)$_2$]. Highlighted in green is the substrate complex.

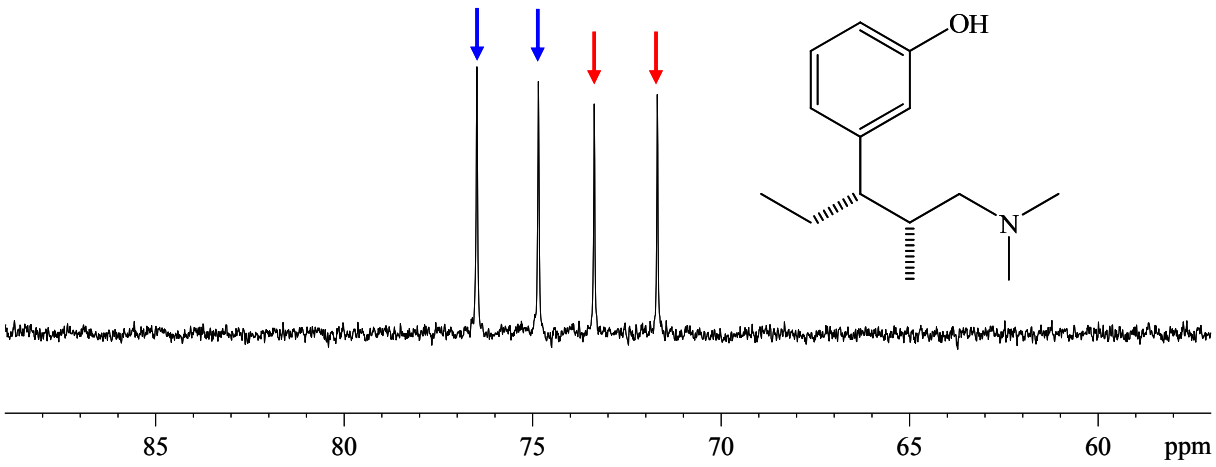

Figure S 14: $^{31}P\{^{1}H\}$-NMR spectrum of a solution of [Rh(DIPAMP)(MeOH-d_4)$_2$][BF_4] and *Z*-3-[1-(dimethylamino)-2-methylpent-2-en-3-yl]phenol (Rh:substrate = ca. 1:10). The arrows indicates the same species as in figure S 13.

Table S 1: $^{31}P\{^{1}H\}$-NMR Data relative to all complexes presented and discussed in this paper.

Ligand (PP)	Type of Complex	Solvent	$^{31}P\{^{1}H\}$-NMR-Data
Me-DuPHOS	$[Rh(PP)(COD)][BF_4]$	MeOH-d_4	δ = 76.4 ppm (d, $J_{P\text{-}Rh}$ = 149.0 Hz)
	$[Rh(PP)(MeOH)_2][BF_4]$	MeOH-d_4	δ = 101.0 ppm (d, $J_{P\text{-}Rh}$ = 204.4 Hz)
	$[Rh_3(PP)_3(\mu_3\text{-}Cl)_2][BF_4]$	acetone-d_6	δ = 96.8 ppm (d, $J_{P\text{-}Rh}$ = 203.1 Hz)
	$[Rh_2(PP)_2(\mu_2\text{-}Cl)_2]$	acetone-d_6	δ = 96.5 ppm (d, $J_{P\text{-}Rh}$ = 199.6 Hz)
	$[Rh_3(PP)_3(\mu_3\text{-}Br)_2][BF_4]$	CH_2Cl_2-d_2	δ = 96.9 ppm (d, $J_{P\text{-}Rh}$ = 204.7 Hz)
	$[Rh_2(PP)_2(\mu_2\text{-}Br)_2]$	CH_2Cl_2-d_2	δ = 97.7 ppm (d, $J_{P\text{-}Rh}$ = 202.2 Hz)
Et-DuPHOS	$[Rh(PP)(MeOH)_2][BF_4]$	MeOH-d_4	δ = 95.0 ppm (d, $J_{P\text{-}Rh}$ = 205.2 Hz)
	$[Rh_2(PP)_2(\mu_2\text{-}Cl)_2]$	THF-d_8	δ = 91.1 ppm (d, $J_{P\text{-}Rh}$ = 199.7 Hz)
Tangphos	$[Rh_3(PP)_3(\mu_3\text{-}Cl)_2][BF_4]$	MeOH-d_4	δ = 120.5 ppm (d, $J_{P\text{-}Rh}$ = 200.9 Hz)
	$[Rh_2(PP)_2(\mu_2\text{-}Cl)_2]$	MeOH-d_4	δ = 102.2 ppm (d, $J_{P\text{-}Rh}$ = 198.0 Hz)
t-Bu-BisP*	$[Rh(PP)(MeOH)_2][BF_4]$	MeOH-d_4	δ = 89.3 ppm (d, $J_{P\text{-}Rh}$ = 205.8 Hz)
	$[Rh_3(PP)_3(\mu_3\text{-}Cl)_2][BF_4]$	MeOH-d_4	δ = 86.8 ppm (d, $J_{P\text{-}Rh}$ = 204.1 Hz)
	$[Rh_3(PP)_3(\mu_3\text{-}OH)_2][BF_4]$	MeOH-d_4	δ = 85.1 ppm (d, $J_{P\text{-}Rh}$ = 196.9 Hz)
	$[Rh_2(PP)_2(\mu_2\text{-}Cl)_2]$	MeOH-d_4	δ = 84.6 ppm (d, $J_{P\text{-}Rh}$ = 199.3 Hz)
DIPAMP	$[Rh(PP)(MeOH)_2][BF_4]$	MeOH-d_4	δ = 80.6 ppm (d, $J_{P\text{-}Rh}$ = 208.1 Hz)
	$[Rh_3(PP)_3(\mu_3\text{-}Cl)_2][BF_4]$	MeOH-d_4	δ = 72.5 ppm (d, $J_{P\text{-}Rh}$ = 203.5 Hz)
	$[Rh_2(PP)_2(\mu_2\text{-}Cl)_2]$	MeOH-d_4	δ = 74.7 ppm (d, $J_{P\text{-}Rh}$ = 199.6 Hz)
	$[Rh_2(PP)_2(\mu_2\text{-}Br)_2]$	acetone-d_6	δ = 76.5 ppm (d, $J_{P\text{-}Rh}$ = 198.7 Hz)
BINAP	$[Rh(PP)(MeOH)_2][BF_4]$	MeOH-d_4	δ = 54.1 ppm (d, $J_{P\text{-}Rh}$ = 205.8 Hz)
	$[Rh_3(PP)_3(\mu_3\text{-}Cl)_2][BF_4]$	MeOH-d_4	δ = 47.2 ppm (d, $J_{P\text{-}Rh}$ = 199.6 Hz)
	$[Rh_2(PP)_2(\mu_2\text{-}Cl)_2]$	CH_2Cl_2-d_2	δ = 49.6 ppm (d, $J_{P\text{-}Rh}$ = 195.5 Hz)

3. Crystallographic Data

Crystal data and details of the structure solution are summarised in table S1. Diffraction data were collected on a STOE-IPDS II diffractometer using graphite monochromated Mo-Kα radiation. The structure were solved by direct methods (SHELXS-97)[1] and refined by full matrix least square techniques against F^2 (SHELXL-97)[1]. XP (Siemens Analytical X-ray Instruments, Inc.) was used for structure representations.

The nonhydrogen atoms, except the not partially occupied atoms of the solvents, were refined anisotropically. The hydrogen atoms were placed into theoretical positions and were refined by using the riding model. The weighting schemes used in the last cycles of refinement are are $\omega = 1/[\sigma^2(Fo^2) + (0.0215P)^2 + 0.0000P]$ for $[Rh_3(t\text{-Bu-BisP*})_3(\mu_3\text{-OH})_2][BF_4]$, $\omega = 1/[\sigma^2(Fo^2) + (0.0182P)^2 + 0.0000P]$ for $[Rh_3((R,R)\text{-Me-DuPHOS})_3(\mu_3\text{-Cl})_2][BF_4]$, $\omega = 1/[\sigma^2(Fo^2) + (0.0230P)^2 + 0.0000P]$ for $[Rh_3((R,R)\text{-}t\text{-Bu-BisP*})_3(\mu_3\text{-Cl})_2][BF_4]$, $\omega = 1/[\sigma^2(Fo^2) + (0.0227P)^2 + 0.0000P]$ for $[Rh_2((R,R)\text{-Et-DuPHOS})_2(\mu_2\text{-Cl})_2]$, $\omega = 1/[\sigma^2(Fo^2) + (0.0353P)^2 + 0.2141P]$ for $[Rh_2((S,S)\text{-Me-DuPHOS})_2(\mu_2\text{-Br}_2)]$, $\omega = 1/[\sigma^2(Fo^2) + (0.0.0202P)^2 + 0.0000P]$ for $[Rh_3((R,R)\text{-Me-DuPHOS})_3(\mu_3\text{-Br})_{0,8}(\mu_3\text{-Cl})_{1,2}][BF_4]$, $\omega = 1/[\sigma^2(Fo^2) + (0.0794P)^2 + 0.0000P]$ for $[Rh_3((R,R)\text{-DIPAMP})_3(\mu_3\text{-Cl})_2][BF_4]$ and $\omega = 1/[\sigma^2(Fo^2) + (0.0000P)^2 + 0.0000P]$ for $[Rh_3((R)\text{-BINAP})_3(\mu_3\text{-Cl})_2][OTf]$.

[1] G. M. Sheldrick, *Acta Cryst. A* **1997** *64*, 112-122.

Table S 2: Crystallographic and refinement data for $[Rh_3(t\text{-Bu-BisP*})_3(\mu_3\text{-OH})_2][BF_4]$, $[Rh_3((R,R)\text{-Me-DuPHOS})_3(\mu_3\text{-Cl})_2][BF_4]$ $[Rh_3((R,R)\text{-}t\text{-Bu-BisP*})_3(\mu_3\text{-Cl})_2][BF_4]$, $[Rh_2((R,R)\text{-Et-DuPHOS})_2(\mu_2\text{-Cl})_2]$, $[Rh_2((S,S)\text{-Me-DuPHOS})_2(\mu_2\text{-Br}_2)]$, $[Rh_3((R,R)\text{-Me-DuPHOS})_3(\mu_3\text{-Br})_{0,8}(\mu_3\text{-Cl})_{1,2}][BF_4]$, $[Rh_3((R,R)\text{-DIPAMP})_3(\mu_3\text{-Cl})_2][BF_4]$ and $[Rh_3((R)\text{-BINAP})_3(\mu_3\text{-Cl})_2][OTf]$.

Compound	$[Rh_3(t\text{-Bu-BisP*})_3(\mu_3\text{-OH})_2][BF_4]$	$[Rh_3((R,R)\text{-Me-DuPHOS})_3(\mu_3\text{-Cl})_2][BF_4]$
Empirical formula	$C_{36}H_{86}BF_4O_2P_6Rh_3$	$C_{54}H_{84}BCl_2F_4P_6Rh_3$
Formula weight	1132.41	1385.47
Crystal system	triclinic	tetragonal
Space group	P*1*	$P2_12_12_1$
a [Å]	12.416(3)	14.483(2)
b [Å]	12.444(3)	14.483(2)
c [Å]	18.186(4)	58.042(12)
α [°]	95.81(3)	90
β [°]	94.37(3)	90
γ [°]	111.98(3)	90
V [$Å^3$]	2572.3(9)	12175(3)
d_c [Mg/m^3]	1.462	1.512
Z	2	8
μ [mm^{-1}]	1.180	1.095
F(000)	1168	5664
Crystal size [mm]	0.25 x 0.22 x 0.20	0.30 x 0.30 x 0.20
Temperature [K]	200	200
Scan range (Θ) [°]	1.78 – 50.00	1.45 – 50.00
Index range (hkl)	-14/14, -14/14, -21/21	-17/17, -17/17, -68/67
Reflection collected	33425	74790
Independent reflections	17398	10153
Observed reflections	14749	8610
parameters	931	631
R1 (int)	0.0253	0.0469
R1 (2σ(I))	0.0256	0.0251
R1 (all data)	0.0324	0.0326
wR2 (all data)	0.0520	0.0432
Goodness of fit	0.971	0.876
Flack parameter	-0.037(16)	-0.029(17)
Largest difference peak and hole (e/ Å)	0.89/-0.56	0.35/-0.35

Compound	$[Rh_3((R,R)$-*t*-Bu-BisP*$)_3$ $(\mu_3$-Cl$)_2][BF_4] \cdot CH_2Cl_2$	$[Rh_2((R,R)$-Et-DuPHOS$)_2$ $(\mu_2$-Cl$)_2]$
Empirical formula	$C_{37}H_{86}BCl_4F_4P_6Rh_3$	$C_{44}H_{72}Cl_2P_4Rh_2$
Formula weight	1254.22	1001.62
Crystal system	triclinic	orthorhombic
Space group	P*1*	$P2_12_12_1$
a [Å]	9.668(2)	14.1975(5)
b [Å]	12.005(2)	16.3823(4)
c [Å]	12.658(3)	20.5561(5)
α [°]	109.83(3)	90
β [°]	94.19(3)	90
γ [°]	90.56(3)	90
V [$Å^3$]	1377.3(5)	4781.1(2)
d_c [Mg/m^3]	1.512	1.391
Z	1	4
μ [mm^{-1}]	1.295	0.964
F(000)	642	2080
Crystal size [mm]	0.35 x 0.20 x 0.10	0.50 x 0.40 x 0.35
Temperature [K]	150	200
Scan range (Θ) [°]	2.11 – 26.16	1.59 – 26.78
Index range (hkl)	-11/11, -14/14, -15/15	-17/17, -20/20, -25/26
Reflection collected	19961	74241
Independent reflections	10467	10133
Observed reflections	9425	9272
parameters	512	469
R1 (int)	0.0195	0.0314
R1 (2σ(I))	0.0236	0.0184
R1 (all data)	0.0274	0.0213
wR2 (all data)	0.0490	0.0381
Goodness of fit	0.991	0.908
Flack parameter	-0.018(18)	-0.029(13)
Largest difference peak and hole (e/ Å)	0.62/-0.35	0.31/-0.27

Compound	$[Rh_2((S,S)\text{-Me-DuPHOS})_2(\mu_2\text{-}Br_2)]$	$[Rh_3((R,R)\text{-Me-DuPHOS})_3(\mu_3\text{-}Br)_{0,8}(\mu_3\text{-}Cl)_{1,2}][BF_4]$
Empirical formula	$C_{36}H_{56}Br_2P_4Rh_2$	$C_{54}H_{84}BBr_{0.80}Cl_{1.20}F_4P_6Rh$
Formula weight	978.33	1421.04
Crystal system	monoclinic	orthorhombic
Space group	$P2_1$	$P2_12_12_1$
a [Å]	11.2912(6)	16.431(3)
b [Å]	16.6047(6)	20.348(4)
c [Å]	11.4464(5)	21.116(4)
α [°]	90	90
β [°]	105.766(4)	90
γ [°]	90	90
V [$Å^3$]	2065.31(16)	7060(2)
d_c [Mg/m^3]	1.573	1.337
Z	2	4
μ [mm^{-1}]	2.912	1.367
F(000)	984	2890
Crystal size [mm]	0.50 x 0.45 x 0.40	0.50 x 0.30 x 0.20
Temperature [K]	200	200
Scan range (Θ) [°]	1.85 – 26.00	1.39 – 25.68
Index range (hkl)	-13/13, -20/20, -14/14	-19/19, -24/24, -25/25
Reflection collected	29726	97567
Independent reflections	8121	13297
Observed reflections	7982	10994
parameters	397	645
R1 (int)	0.0292	0.0521
R1 (2σ(I))	0.0198	0.0229
R1 (all data)	0.0204	0.0321
wR2 (all data)	0.0500	0.0430
Goodness of fit	1.040	0.769
Flack parameter	0.031(4)	-0.003(9)
Largest difference peak and hole (e/ Å)	0.47/-0.71	0.44/-0.58

Compound	$[Rh_3((R,R)\text{-DIPAMP})_3(\mu_3\text{-}Cl)_2][BF_4] \cdot CH_2Cl_2$	$[Rh_3((R)\text{-BINAP})_3(\mu_3\text{-}Cl)_2][OTf] \cdot 2\ CH_2Cl_2$
Empirical formula	$C_{85}H_{86}BCl_4F_4O_6P_6Rh_3$	$C_{135}H_{100}Cl_6F_3O_3P_6Rh_3S$
Formula weight	1926.70	2566.46
Crystal system	triclinic	monoclinic
Space group	P*1*	P2_1
a [Å]	13.136(3)	16.493(3)
b [Å]	13.405(3)	23.276(5)
c [Å]	14.779(3)	16.775(3)
α [°]	85.58(3)	90
β [°]	68.44(3)	118.10(3)
γ [°]	68.06(3)	90
V [Å^3]	2239.6(8)	5681(2)
d_c [Mg/m^3]	1.429	1.500
Z	1	2
μ [mm^{-1}]	0.830	0.736
F(000)	978	2608
Crystal size [mm]	0.50 x 0.30 x 0.30	0.20 x 0.15 x 0.10
Temperature [K]	200	200
Scan range (Θ) [°]	1.49 – 23.50	2.82 – 53.48
Index range (hkl)	-14/14, -15/15, -16/16	-19/19, -27/27, -19/19
Reflection collected	12727	48333
Independent reflections	12727	20002
Observed reflections	10558	9698
parameters	669	1393
R1 (int)	0.0000	0.0899
R1 (2σ(I))	0.0530	0.0424
R1 (all data)	0.0611	0.1018
wR2 (all data)	0.1332	0.0745
Goodness of fit	1.017	0.554
Flack parameter	0.00(4)	-0.01(2)
Largest difference peak and hole (e/ Å)	1.15/-0.71	0.83/-0.54